Bull. Chem. Soc. Ethiop. **2023**, 37(6), 1553-1564.
DOI: https://dx.doi.org/10.4314/bcse.v37i6.19

ISSN 1011-3924
Printed in Ethiopia
Online ISSN 1726-801X

FABRICATION OF NOVEL PN-HETEROJUNCTION CuS/TiO_2 NANOCOMPOSITE FOR THE PHOTOCATALYTIC DEGRADATION OF RHODAMINE B DYE UNDER VISIBLE LIGHT IRRADIATION

Zahid Mahmood[1*], Waheed Aslam[2], Muhammad Bilal[1] and Khalid Javed[1]

[1]Institute of Chemical Sciences, Bahauddin Zakariya University, Multan 60800, Punjab, Pakistan
[2]Department of Physics, University of Sargodha, Pakistan

(Received May 7, 2022; Revised May 29, 2023; Accepted July 24, 2023)

ABSTRACT. In the current study, a novel visible light-active photocatalyst CuS/TiO_2 nanocomposite was synthesized by a template-free hydrothermal method. Fourier transform infrared spectroscopy (FTIR) confirmed the formation of synthesized nanocomposites and the structural characteristics of synthesized nanoparticles were characterized and confirmed by the X-ray diffraction (XRD) technique. The morphology and particle size of synthesized nanocomposites were measured by a field emission scanning electron microscope (FESEM), which revealed an average particle size of around 30 nm. The optimized efficiency of the fabricated photocatalyst was assessed for the photodegradation of rhodamine B (RhB) dye. It was observed that the photodegradation efficiency of CuS/TiO_2-Y composites having a molar ratio of 1:1 for RhB was found to be 89.54% under visible light irradiation.

KEY WORDS: CuS/TiO_2 nanocomposite, Heterojunction structure, Rhodamine B, Photodegradation, Visible light irradiation

INTRODUCTION

Organic dyes are widely used in the manufacturing of textiles and food. Being highly toxic and non-biodegradable to aquatic life and carcinogenic effect on humans, organic dyes are considered an important pollutant source to the environment [1]. The presence of dyes in wastewater is a considerable environmental issue and their removal is a big challenge [2, 3]. RhB is one of the organic dyes which completely dissolved in water and is widely used in textile, printing, paper, food, and pharmaceutical products. It has a damaging effect on the eyes, skin, and respiratory system [4, 5].

Various techniques such as adsorption, chemical precipitation, coagulation, flocculation, membrane filtration, and biodegradation have been employed to remove the organic pollutants from water [6]. Amongst these, photocatalysis is one of the most important techniques for the generation of green energy and the decomposition of many organic pollutants from water [7, 8]. The photocatalytic degradation technique has high efficiency in the mineralization of organic pollutants, producing H_2O, CO_2, and inorganic mineral ions as end products [9, 10]. N-type TiO_2 is considered the most effective photocatalyst for artificial photosynthesis due to its superior properties such as high photo-corrosion resistance, durability, strong oxidizing power, low cost, and low toxicity [11-13].

The bandgap of TiO_2 is 3.2 eV and it is active in the ultraviolet region when expose to solar radiation [14]. The visible light irradiation with a wavelength range (400-800 nm) is unable to overcome the bandgap of TiO_2 and thus separation of holes and electrons is not possible [15]. This limitation of TiO_2 makes it unable to utilize 43% of the solar spectrum and thus solar-induced reactions are not possible [16]. Some suitable arrangements are necessary to obtain better results under solar light irradiation by TiO_2. A heterostructure obtained by loading metal sulfides or metal oxides on the surface of TiO_2 and the prepared nanomaterial showed improved visible light harvesting [17, 18]. Zhang *et al.* used the solvothermal method for the preparation of TiO_2/Cu_2O heterostructure nanoparticles. Hydrogen production level is enhanced with the loading of Cu_2O on TiO_2 [19]. Yadav *et al.* used the hydrothermal method for the synthesis of TiO_2/CdS NCs [20]. Swaminathan *et al.*

*Corresponding author. E-mail: zdry39@gmail.com

prepared AgBr/TiO_2 NCs by deposition method and found better results for the degradation of RR120 [21].

The low band gap of CuS made it a promising candidate among other metal sulfides. P-type semiconductor, CuS with a small band gap of 2.1 eV can easily be integrated with N-type TiO_2 to be used in photocatalysis [22]. Additionally, CuS is non-toxic, stable, and has distinctive physicochemical properties making it a favorable choice for coupling with TiO_2 to improve photocatalytic properties [23, 24].

The present study aimed to synthesize CuS/TiO_2 nanocomposites using a template-free hydrothermal method and investigate their ability to photodegrade RhB dye under visible light irradiation. Herein, a large bandgap semiconductor TiO_2 is coupled with a small bandgap semiconductor CuS to form a PN-heterojunction structure. The synthesized NCs showed better results for visible light absorptivity due to the mobility of charge carriers and reduced the recombination of electron-hole pairs [25, 26].

EXPERIMENTAL

Preparation of nanocomposites of CuS/TiO_2

The temple-free hydrothermal method was employed for the synthesis of TiO_2, CuS NPs, and CuS/TiO_2 NCs. Titanium tetra-isopropoxide titanium tetra Ti[$OCH(CH_3)_2$]$_4$ (TTIP), $Na_2S.9H_2O$, $Cu(NO_3)_2.2H_2O$, and KOH were used along with deionized (DI) water. All these chemicals were of analytical grades and purchased from Sigma Aldrich for the synthesis of TiO_2, CuS NPs, and Cus/TiO_2 NCs.

To prepare TiO_2 NPs, 10 mL of 0.02 M solution of KOH was mixed with 30 mL of 0.05 M solution of TTIP and then stirred for 20 min at 65 °C to get a homogenous and clear solution. This solution was put into a 60 mL Teflon autoclave, then heated at 190 °C for 24 hours in the oven to get TiO_2 NPs. After that Autoclave was cool down to room temperature and then the synthesized material was taken out and washed with water and ethanol. In order to remove the moisture and other impurities, the final washed product was vacuum dried at 70 °C for seven hours.

To prepare CuS NPs, 0.05M solution of $Na_2S.9H_2O$ and 0.05 M solution of $Cu(NO_3)_2.2H_2O$ were prepared separately. Then 15 mL of as-prepared solutions were mixed by slow stirring. 10 mL of 0.02 M solution of KOH was added dropwise and stirred for 10 min. The whole mixture was transferred to an autoclave and heated at 190 °C for 24 hours to obtain CuS NPs. After that autoclave was cool down to room temperature and then the synthesized material was taken out and washed with water and ethanol. In order to remove the moisture and other impurities, the final washed product was vacuum dried at 70 °C for seven hours.

CuS/TiO_2 NCs were synthesized by mixing and stirring already prepared solutions of CuS and TiO_2 NPs. This solution was transferred to the Teflon autoclave and headed at 190 °C for 24 hours. Then synthesized material was washed with water and ethanol and then vacuum dried at 70 °C for seven hours. Herein, a series of NCs of CuS/TiO_2 were synthesized according to the molar ratio of CuS/TiO_2-X (0.5:1), CuS/TiO_2-Y (1:1), and CuS/TiO_2-Z (2:1).

Characterization

XRD analysis for synthesized TiO_2, CuS NPs, and CuS/TiO_2 NCs was done by Shimadzu XRD-7000S to characterize the structural aspects. The morphologies of the prepared materials were analyzed by FESEM (Nova Nano FESEM 450). The infrared absorption spectra of the prepared materials were detected by FTIR spectrophotometer (Nicolet 10). Diffuse reflective spectroscopy (DRS) studies and bandgap calculation for NPs and NCs were done by UV-Vis spectroscopy at room temperature (Shimadzu Corporation).

Photocatalytic activity

A series of experiments were done to check the photocatalytic performance of CuS, TiO_2 NPs, and CuS/TiO_2 NCs for the degradation of RhB dye. Experimentally, 60 mg/L solution of RhB was prepared in DI water, then 0.05 g catalyst was added to 20 mL RhB solution. The suspension was kept under constant stirring for 20 min in the dark condition to get the adsorption/desorption equilibrium between the RhB solution and the catalyst. Then, the suspension was put under the Xenon lump (1000W) as a light source and stirred constantly. After the time interval of 15 min, 5 mL suspension was taken out and centrifuged. The degradation of RhB dye was checked by a UV-Vis spectrophotometer. Through preliminary photocatalytic activities of different prepared ratios NCs, it was noted that CuS/TiO_2 –Y (1:1) showed better photocatalytic activity.

RESULTS AND DISCUSSION

FTIR spectrum of CuS/TiO_2 nanocomposites

Figure 1 shows the FTIR spectra of TiO_2, CuS NPs, and CuS/TiO_2 NCs. The FTIR spectrum of TiO_2 and CuS/TiO_2 NCs typically exhibits a Ti-OH stretching mode at around 1380 cm^{-1}. Additionally, asymmetrical and symmetrical stretching vibrations of the hydroxyl group (-OH) can be observed at approximately 3200 cm^{-1} [27].

The absorption band of CuS and CuS/TiO_2 NCs observed at 1631 cm^{-1} in the spectrum can be attributed to the OH bending mode of water. The band located at 1112 cm^{-1} can be attributed to the asymmetric stretching mode of the carbonyl (C=O) group [28]. The observed absorption band at 1112 cm^{-1} and 1631 cm^{-1} are related to the characteristic absorption peak of CuS. It demonstrated the successful composite formation of CuS/TiO_2 NCs.

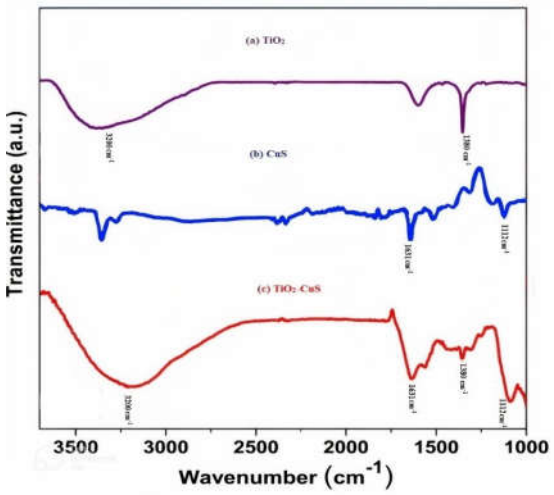

Figure 1. FTIR analysis of (a) TiO_2 NPs, (b) CuS NPs and (c) CuS/TiO_2 NCs.

Morphology and composition analysis

XRD patterns of CuS, TiO_2 NPs, and CuS/TiO_2 NCs are illustrated in Figure 2. It can be seen from the XRD pattern that all the diffraction peaks related to NPs of CuS are corresponding to the hexagonal CuS {JCPDS # 06-0464} [29] and entire diffraction peaks of NPs of TiO_2 are identical to the anatase

form of TiO_2 {JCPDS # 21-1272} [30]. For the three different prepared NCs of CuS/TiO_2, the diffraction peaks appear at 29.2°, 32.8°, and 47.9° which correspond to CuS NPs, which revealed that CuS nanoparticles have been effectively aggregated with TiO_2. The XRD diffraction peaks of TiO_2 NPs in the prepared composites are continuously increased by continuously decreasing the loading of CuS over TiO_2 NPs, so the CuS is continuously weakened. The absence of any noticeable peak shift in the FTIR pattern of CuS/TiO2 NCs indicates that the composites are composed solely of CuS and TiO_2 NPs. So, this is an already established fact that there is no structural stress or lattice strain in the doped materials [31].

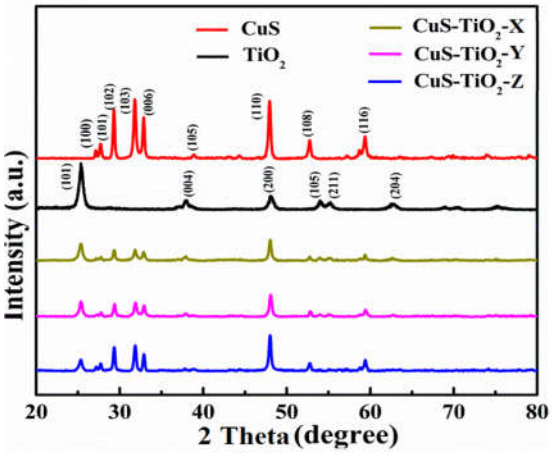

Figure 2. XRD patterns of CuS, TiO_2 NPs, and NCs of CuS/TiO_2 -X, CuS/TiO_2 -Y, CuS/TiO_2 –Z.

FESEM images of the photocatalyst

FESEM is used for the morphological analysis of the synthesized materials. For the effective photocatalytic functioning of synthesized materials, a large surface area is required that can only be possible if the growth of particles would be nanosized. The FESEM images of CuS, TiO_2 NPs, and CuS/TiO_2 NCs are seen in Figure 3.

FESEM images revealed that the grain size of all three materials was ranging from 25 nm to 35 nm. Nano-sized particles of the synthesized materials have a wide surface area for exposure to photons in solar radiation.

Bandgap calculation by UV-Visible spectrophotometry

Bandgap shows an important role in the photocatalytic performance of semiconductors. The bandgap for the synthesized NCs of CuS/TiO_2 was calculated by UV-Visible spectrophotometry in visible light (400 nm to 800 nm). Tauc relationship was used for bandgap calculation which is given as:

$(\alpha h\nu) = A(h\nu - Eg)n$

where α indicates the absorption coefficient, hν is the photon energy, while Eg is the bandgap of incident radiations. The UV-Visible spectrum of CuS/TiO_2-Y under visible light and its calculated bandgap (2.5 eV) is shown in Figure 4.

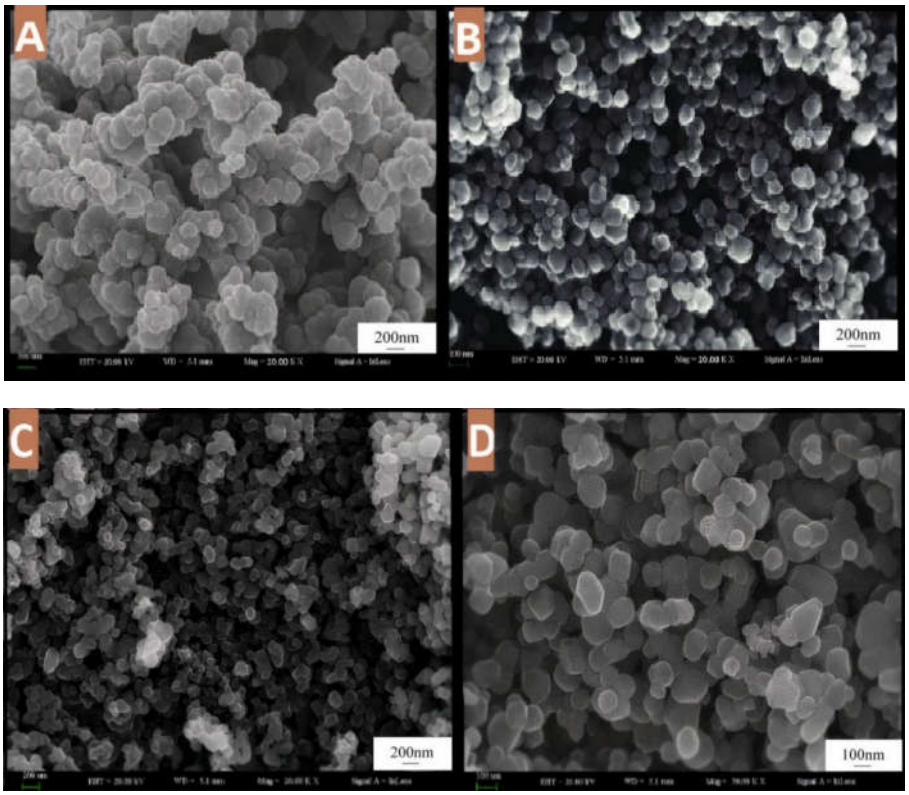

Figure 3. FESEM images for different samples, (A) pure CuS NPs, (B) pure TiO_2 NPs, (C) CuS/TiO_2 NCs and (D) high-resolution FESEM images of CuS/TiO_2 NCs.

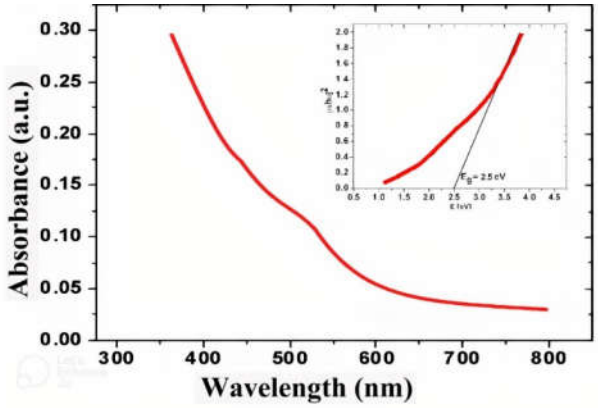

Figure 4. UV-Vis spectrum under visible light and bandgap calculation for CuS/TiO_2 NCs.

UV-Visible DRS analysis

The light-harvesting ability of the synthesized materials was evaluated by the DRS technique, as shown in Figure 5. Here is the comparison of bared CuS, TiO_2 NPs, and various prepared NCs of CuS/TiO_2 presented, after light absorption takes place in the visible region. It can be seen from Figure 5, that as the loading of CuS on TiO_2 is increased, the absorption intensity also gradually increased. So, results showed that the loading of CuS NPs improves the visible light harvesting of TiO_2 which ultimately enhanced the performance of the Cus/TiO_2 NCs.

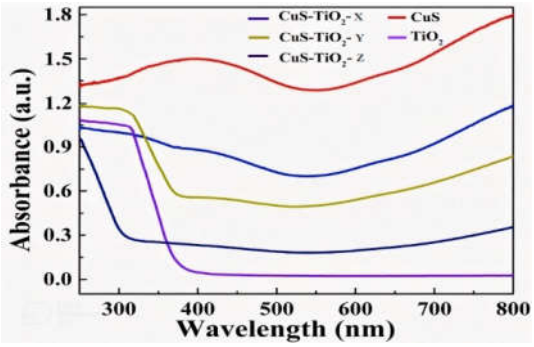

Figure 5. DRS of CuS, TiO_2 NPs, and various prepared CuS/TiO_2 NCs.

Photocatalytic degradation of the organic pollutant

Photocatalytic activities of samples under visible light absorption are shown in Figure 6. The photocatalytic degradation performance was calculated by the equation given below;

$$\% \text{ degradation} = (C_0 - C_t)/C_0 \times 100\% \quad (1)$$

Here C_0 refers to the initial time of absorption, and C_t represents the absorption after various time intervals (0, 30, 60, 90, 120, 150, and 180 min).

The rate of self-degradation of RhB dye under visible light was poor without any photocatalyst. The activity of CuS/TiO_2 NCs increased as compared to bare TiO_2 NPs. Amongst all the synthesized NCs, the CuS/TiO_2-Y (1:1) nanocomposite gave the best performance to degrading RhB dye under the same conditions. Additionally, a further increase in the mass ratio of CuS NPs over TiO_2 by more than 50% does not cause any significant increase in photocatalytic activity as shown in Figure 7.

Comparison of the photocatalytic activities

The photocatalytic performance of synthesized NPs and NCs under visible light irradiation was examined by the Xenon lamp system as shown in Figure 8. The results showed that the absorbance of the dye solution gradually decreased with time. TiO_2 NPs showed low photocatalytic efficiency due to a larger band gap (3.2 eV) that makes it unable to absorb light in the visible region. The maximum photodegradation efficiency of TiO_2 NPs was approximately 47.94% at 670 nm after 180 min. The photodegradation efficiency of CuS NPs was approximately 59.09% at 670 nm which might be due to its narrow band gap (2.1 eV). Furthermore, CuS/TiO_2-Y NC has shown maximum photodegradation efficiency (89.54%) at the same wavelength. The CuS/TiO_2-Y NC showed a better photodegradation efficiency than the bare CuS and TiO_2 NPs which might be due to the efficient charge separation and lowering recombination rate of electron-hole pairs [32].

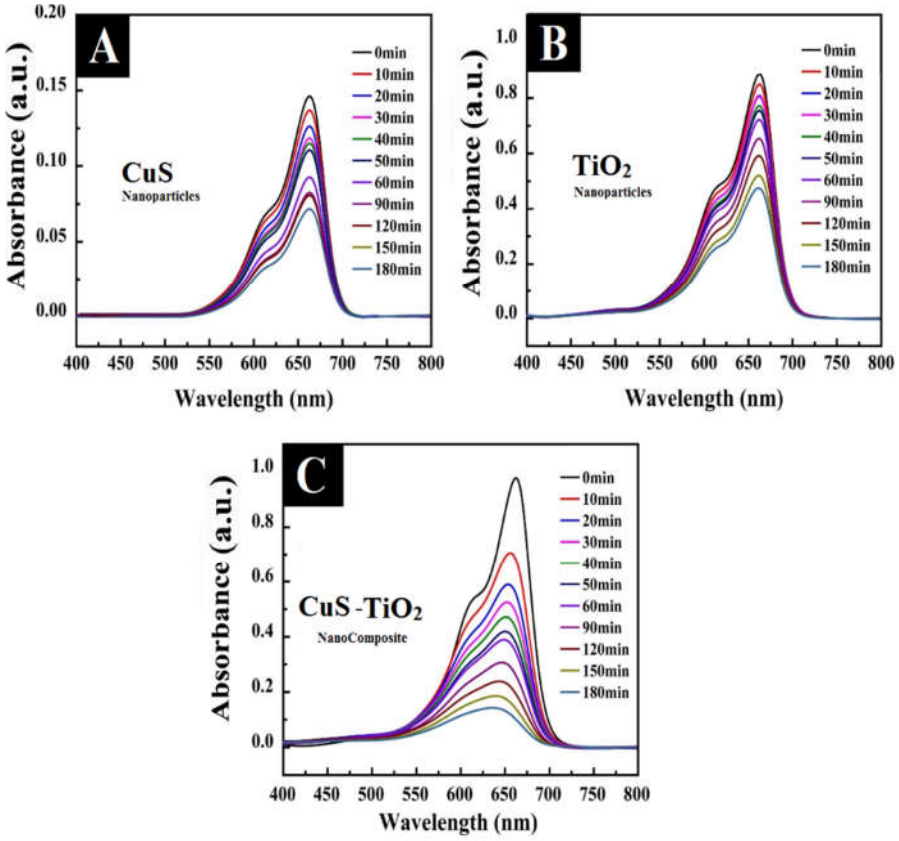

Figure 6. Photodegradation of RhB dye under visible light by (a) CuS NPs, (b) TiO_2 NPs and (c) CuS/TiO_2 NC.

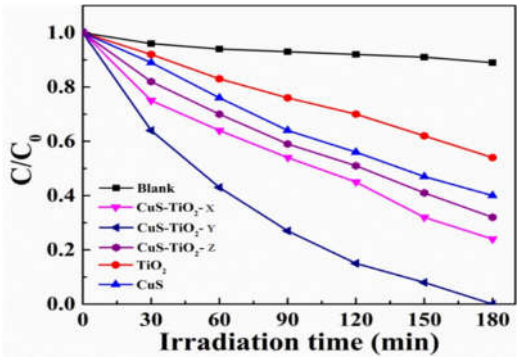

Figure 7. The photocatalytic activity of CuS, TiO_2 NPs, and various CuS/TiO_2 NCs for degradation of RhB under visible light irradiation.

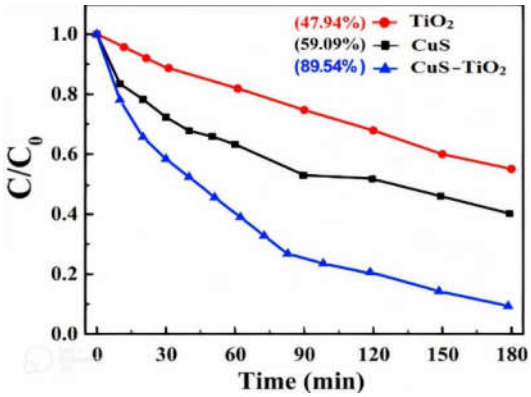

Figure 8. Comparison of Photodegradation of RhB for CuS, TiO_2 NPs, and CuS-TiO_2 NCs.

Reusability of the photocatalyst

To access the activity of photocatalysts, reusability is one of the most important parameters. CuS/TiO_2-Y NC were analyzed for degradation of RhB dye over four successive runs, each run takes 120 min as shown in Figure 9. The efficiency of the under-consideration sample was reduced to 7% after four successive cycles. This minor reduction showed the excellent photocatalytic performance and stability of CuS/TiO_2-Y NC to degrade RhB dye, under visible light irradiation.

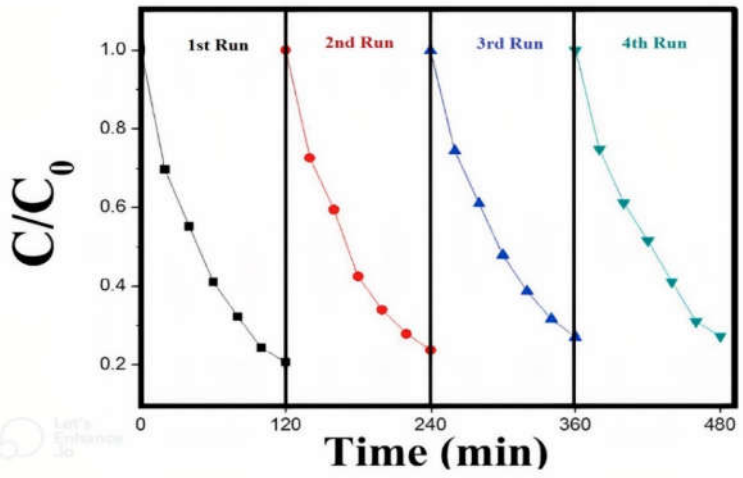

Figure 9. Effect of reusability on removal efficiency of CuS/TiO_2-Y NC for RhB.

Schematic mechanism of PN-heterojunction structure of CuS/TiO_2 NCs

The band gap is an important aspect to investigate the photocatalytic properties of semiconductors under solar light irradiation. TiO_2 is an N-type semiconductor and its band gap is 3.2 eV while CuS is a P-type semiconductor having a band gap of 2.1 eV.

TiO_2 is a very stable photocatalyst, has a wide band gap, and can only be activated under ultraviolet illumination. On the other hand, CuS has a shorter band gap semiconductor, with the advantage of visible light activation, and has a problem with electron-hole recombination. The loading of CuS over TiO_2 produces a P-N junction heterostructure at the interface of semiconductors, which results in suppressing the electron-hole recombination rate. Due to the small bandgap of CuS, it has a different NHE (Normal Hydrogen Electrode) potential compared with TiO_2, causing a reduction in the band gap of CuS/TiO_2 by introducing a new Fermi level within the bandgap as depicted in Figure 10(A). The P-N heterojunction is formed at the interface of these P and N-type semiconductors. Electron-hole pairs which are produced in CuS NPs are the reason for the disturbance of the equilibrium which results in the transfer of electrons to the CB and creates holes in the VB of TiO_2. This effective separation of holes and electrons results in improved photocatalytic efficiency of the synthesized composites. Due to the improved bandgap of CuS/TiO_2 (2.5 eV), it showed better photocatalytic activity under visible light irradiation, as illustrated in Figure 10(B).

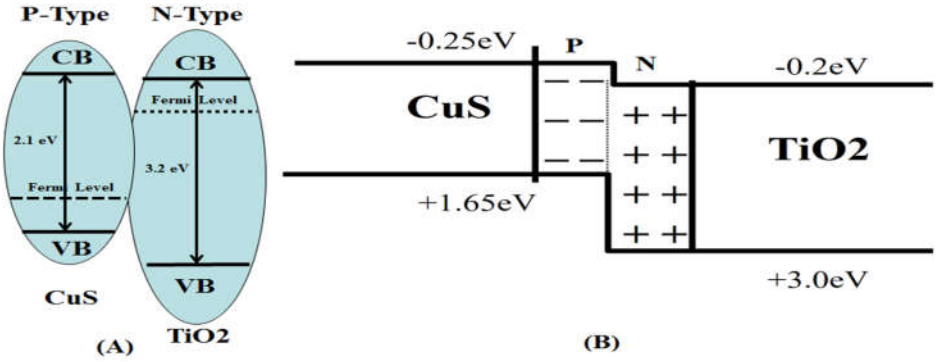

Figure 10. (A) and (B) Schematic diagram for CuS/TiO_2 NCs.

Proposed photocatalytic degradation mechanism of RhB

Based on the charge separation, photocatalytic degradation of RhB dye by CuS/TiO_2-Y NC will be following the reaction mechanism as given below;

$$CuS + h\nu \rightarrow CuS\ (e^{-}CB + h^{+}\ VB)$$

$$CuS\ (e^{-}CB) + TiO_2 \rightarrow CuS + TiO_2\ (e^{-}CB)$$

$$TiO_2\ (e^{-}CB + O_2) \rightarrow TiO_2 + O_2^{\cdot-}$$

$$O_2^{\cdot-} + H_2O \rightarrow HO_2^{\cdot-} + OH^{-}$$

$$HO_2^{\cdot-} + H_2O \rightarrow OH + OH^{-}$$

$$H_2O_2 \rightarrow 2OH^{\cdot}$$

$$TiO_2\ (h^{+}\ VB + H_2O) \rightarrow H^{+} + OH^{-}$$

$$TiO_2\ (h^{+}\ VB + OH^{-}) \rightarrow OH^{\cdot}$$

$$RhB + OH^{\cdot} + O_2^{\cdot-} \rightarrow H_2O + CO_2\ \text{(degradation products)}$$

When electrons are excited from VB to CB of CuS, electrons are created in the CB and the holes are created in the VB. On decreasing potential energy, the CB electrons of CuS are transferred to the CB of TiO_2, whereas the holes from VB of CuS are moved to VB of TiO_2. The anions of superoxide ($O_2^{\bullet -}$) radical are formed when molecular oxygen is present in the dissolved water and captured the CB electrons of TiO_2, which results in the formation of OH• radicals. The holes present in VB of TiO_2 undergo reactions with OH^- or H_2O molecules, leading to their oxidation and formation of hydroxyl radicals (OH•). In addition to hydroxyl radicals (OH•), superoxide radical anions ($O_2^{\bullet -}$) have also been found to contribute to the photocatalysis of RhB dye, which is identified by scavengers test. These species work together to break down the RhB molecule into smaller and harmless substances.

CONCLUSION

Nanoparticles of CuS, TiO_2, and nanocomposites of CuS/TiO_2 were prepared by template-free hydrothermal method. The synthesized nanoparticles were characterized by XRD. The morphology and particle size of synthesized nanoparticles were measured by FESEM, which revealed an average particle size of around 30 nm. Furthermore, the UV-Visible spectroscopy technique is used for band gap studies and photodegradation analysis under visible light illumination. The low bandgap of P-type CuS (2.1 eV) decreased the bandgap of TiO_2 (3.2 eV), so synthesized nanocomposites of CuS/TiO_2-Y(1:1) showed band gap contraction (2.5 eV), which makes the material photoactive against RhB (a model contaminant) under the visible region of the spectrum. The catalytic degradation efficiency reached a maximum (89.54%) under visible light irradiation when the molar ratio of CuS/TiO_2-Y NC was 1:1. The enhanced photocatalytic activity of CuS/TiO_2-Y NC might be due to the lowering of the recombination rate of electron-hole pairs, efficient separation and transfer of charge carriers. The reusability of synthesized CuS/TiO_2-Y NC was analyzed for four successive cycles which showed reduced efficiency up to 7% only. The better degradation efficiency, environmental compatibility, easy handling, reusability, and recovery of the photocatalyst make this nanocomposite suitable for industrial applications.

REFERENCES

1. Papic, S.; Koprivanac, N.; Bozic, A.; Metes, M. Removal of some reactive dyes from synthetic wastewater by combined Al(III) coagulation/carbon adsorption process. *Dyes Pigm*. **2004**, 62, 291-298.
2. Di, L.; Yang, H; Xian, T.; Chen, X. Construction of Z-scheme g-C_3N_4/CNT/$Bi_2Fe_4O_9$ composites with improved simulated-sunlight photocatalytic activity for the dye degradation. *Micromachines* **2018**, 9, 613.
3. Jiang, R.; Zhu, H.; Fu, Y.; Jiang, S.; Zong, E.; Yao, J. Photocatalytic decolorization of Congo red wastewater by magnetic $ZnFe_2O_4$/graphene nanosheets composite under simulated solar light irradiation. *Ozone Sci. Eng*. **2020**, 42, 174-182.
4. Mittal, A.; Malviya, A.; Kaur, D. Studies on the adsorption kinetics and isotherms for the removal and recovery of methyl orange from wastewaters using waste materials. *J. Hazard. Mater.* **2007**, 148, 229-240.
5. Richardson, D.; Willson, S; Rusch, A. Use of rhodamine water tracer in the marshland upwelling system. *Ground Water* **2004**, 42, 678-688.
6. Liang, Z.; Yan, F.; Rtimi, S.; Bandara, J. Piezoelectric materials for catalytic/photocatalytic removal of pollutants: recent advances and outlook. *Appl. Catal. B Environ*. **2019**, 241, 256-269.
7. Wang, G.; Liu, S.; He, T.; Liu, X.; Deng Q.; Mao Y.; Wang S. Enhanced visible-light-driven photocatalytic activities of $Bi_2Fe_4O_9$/g-C_3N_4 composite photocatalysts. *Mater. Res. Bull*. **2018** 104, 104-111.

8. Qourzal, S.; Barka, N.; Tamimi, M. Photodegradation of 2-Naphthol in water by artificial light illumination using TiO_2 photocatalyst: Identification of intermediates and the reaction pathway. *Appl. Catal. A: General* **2008**, 334, 386-393
9. Taleb, A. Adsorption and photocatalytic degradation of 2-CP in wastewater onto CS/$CoFe_2O_4$ nanocomposite synthesized using gamma radiation. *Carbohydr. Polym*. **2014**, 114, 65-72.
10. Hong, Y.; Ren, A.; Jiang, Y. Sol-gel synthesis of visible-light-driven Ni(1−x)-Cu(x)Fe_2O_4 photocatalysts for degradation of tetracycline. *Ceram. Int.* **2015**, 41, 1477-1486.
11. Hu, Y.; Yuan, C. Low-temperature preparation of photocatalytic TiO_2 thin films from anatase sols. *J. Crystal Growth*. **2005**, 274, 563-568.
12. Ali, A.; Oh, C. Photocatalytic performance of CoS_2-Graphene-TiO_2 ternary composites for reactive black B (RBB) degradation. *J. Korean Cream. Soc*. **2017**, 54, 308-313.
13. Min, S.; Hou, J.; Lei, Y.; Ma, X.; Lu, G. Facile one-step hydrothermal synthesis toward strongly coupled TiO_2/graphene quantum dots photocatalysts for efficient hydrogen evolution. *Appl. Surf. Sci*. **2017**, 396, 1375-1382.
14. Kang, S.; Pawar, C.; Park, J.; Kim, G.; Ahn, H.; Lee, S. Minimization of recombination losses in 3D nanostructured TiO_2 coated with few layered g-C_3N_4 for extended photo-response. *J. Korean Cream. Soc.* **2016**, 53, 393-399.
15. Ding, D.; Liu, K.; He, S.; Gao, C.; Yin, Y. Ligand-exchange assisted formation of Au/TiO_2 Schottky contact for visible-light photocatalysis. *Nano Lett.* **2014**, 14, 6731-6736.
16. Sang, Y.; Zhao, Z.; Tian, J.; Hao, P.; Jiang, H.; Liu, H.; Claverie, P. Enhanced photocatalytic property of reduced graphene oxide/TiO_2 nanobelt surface heterostructures constructed by an in situ photochemical reduction method. *Small*. **2014**, 10, 3775-3782.
17. Khanchandani, S.; Srivastava, K.; Kumar, S.; Ghosh, S.; Ganguli, K. Band gap engineering of ZnO using core/shell morphology with environmentally benign Ag_2S sensitizer for efficient light-harvesting and enhanced visible-light photocatalysis. *Inorg. Chem*. **2014**, 53, 8902-8912.
18. Xu, H.; Shang, H.; Wang, C.; Jin, L.; Chen, C.; Wang, C.; Du, Y. Three-dimensional open $CoMoO_x$/$CoMoS_x$/CoS_x nano box electrocatalysts for efficient oxygen evolution reaction. *Appl. Catal. B: Environ.* **2020**, 118605.
19. Hu, Q.; Ren, T.; Deng, D.; Xu, L.; Chen, J.; Xiao, Y.; He, P. Constructing carbon microspheres/$MnFe_2O_4$/g-C_3N_4 composite photocatalysts for enhanced photocatalytic activity under visible light irradiation. *Inorg. Chem. Commun.* **2021**, 134, 108947.
20. Tian, Y.; Chang, B.; Yang, Z.; Zhou, B.; Xi, F.; Dong, X. Graphitic carbon nitride–$BiVO_4$ heterojunctions: simple hydrothermal synthesis and high photocatalytic performances. *RSC Adv.* **2014**, 4, 4187-4193.
21. Yeo, C.; Kang, C. Preparation of WO_3-TiO_2 photocatalyst and evaluation of its photo-activity in the visible light range. *J. Kor. Powd. Met. Inst*. **2013**, 20), 474-478.
22. Lu, Y.Y.; Zhang, Y.Y.; Zhang, J.; Shi,Y.; Li, Z.; Feng Z.C.; Li, C. In situ loading of CuS nanoflowers on rutile TiO_2 surface and their improved photocatalytic performance. *Appl. Surf. Sci.* **2016**, 370, 312-319.
23. Shi, Y.; Chen, Y.; Tian, G.; Wang, L.; Xiao, Y.; Fu, H. Hierarchical Ag/Ag_2S/CuS ternary heterostructure composite as an efficient visible-light photocatalyst. *ChemCatChem*. **2015**, 7, 1684-1690.
24. Figueroa, A.; Alvarez, M.; Cruz, S.; Contreras, G.; Torres, A.; Hernández, F.; Arrocena, A. Nanomaterials made of non-toxic metallic sulfides: A systematic review of their potential biomedical applications. *Mater. Sci. Eng. C* **2017**, 76, 1305-1313.
25. Liu, S.; Yu, J.; Jaroniec, M. Tunable photocatalytic selectivity of hollow TiO_2 microspheres composed of anatase polyhedra with exposed {001} facets. *J. Am. Chem. Soc.* **2010**, 132, 11914-11916.
26. Agboola, O.; Shakir, I.; Haider, S. Development of internal electric field induced $NiFe_2O_4$/CdO p-n nano-heterojunctions for solar light activated photodegradation of methylene blue dye. *Ceram. Int.* **2022**, 48, 13572-13579.

27. Lakkanna, C.; Yatnatti, M.; Linganagoudar, R.; Ravindra, K.; Kadadevarmath, J. A simple approach on synthesis of TiO_2 nanoparticles and its application in dye sensitized solar cells. *J. Nano-Electron. Phys*. **2017**, 9, 04005-1-04005-6.
28. Riyaz, S.; Parveen, A.; Azam, A. Microstructural and optical properties of CuS nanoparticles prepared by sol-gel route. *Perspect. Sci.* **2016**, 8, 632-635.
29. Dutta, S.; Ray, C.; Mallick, S.; Sarkar, S.; Sahoo, R.; Negishi, Y.; Pal. T. A gel-based approach to design hierarchical CuS decorated reduced graphene oxide nanosheets for enhanced peroxidase-like activity leading to colorimetric detection of dopamine. *J. Phys. Chem. C.* **2015**, 119, 23790-23800.
30. Bao, N.; Yin, Z.; Zhang, Q.; He, S.; Hu, X.; Miao, X. Synthesis of flower-like monoclinic $BiVO_4$/surface rough TiO_2 ceramic fiber with heterostructures and its photocatalytic property. *Ceram. Int.* **2016**, 42, 1791-1800.
31. Moumita, C.; Kousik, B.; Debabrata, P. Controlled synthesis of CuS/TiO_2 heterostructured nanocomposites for enhanced photocatalytic hydrogen generation through water splitting. *J. Am. Chem. Soc.* **2018**, 57, 4524-4533.
32. Hamed, R.; Faranak, M. Immobilization of mixed cobalt/nickel metal-organic framework on a magnetic $BiFeO_3$: A highly efficient separable photocatalyst for degradation of water pollutions. *J. Photochem. Photobiol. A: Chem.* **2017**, 41, 1016.